applied sciences

MDPI

Article

Modeling Heat Transport in Systems of Hydrate-Filled Sediments Using Residual Thermodynamics and Classical Nucleation Theory

Mojdeh Zarifi [1,*], Bjørn Kvamme [2] and Tatiana Kuznetsova [1]

[1] Department of Physics and Technology, University of Bergen, Allegaten 55, 5007 Bergen, Norway; tatyana.kuznetsova@uib.no
[2] Hyzen Energy, 26701 Quail Creek, Laguna Hills, CA 92656, USA; Bkvamme@hyzenenergy.com
* Correspondence: mojdeh.zarifi@uib.no; Tel.: +47-416-45-284

Abstract: As in any other phase transition, hydrate phase transition kinetics involves an implicit coupling of phase transition thermodynamic control and the associated dynamics of mass and heat transport. This work provides a brief overview of certain selected hydrate film growth models with an emphasis on analyzing the hydrate phase transition dynamics. Our analysis is based on the fundamental properties of hydrate and hydrate/liquid water interfaces derived from molecular modeling. We demonstrate that hydrate phase transitions involving water-dominated phases are characterized by heat transport several orders of magnitude faster than mass transport, strongly suggesting that any hydrate phase transition kinetic models based on heat transport will be entirely incorrect as far as thermodynamics is concerned. We therefore propose that theoretical studies focusing on hydrate nucleation and growth should be based on concepts that incorporate all the relevant transport properties. We also illustrate this point using the example of a fairly simplistic kinetic model, that of classical nucleation theory (CNT), modified to incorporate new models for mass transport across water/hydrate interfaces. A novel and consistent model suitable for the calculation of enthalpies is also discussed and appropriate calculations for pure components and relevant mixtures of carbon dioxide, methane, and nitrogen are demonstrated. This residual thermodynamic model for hydrate is consistent with the free energy model for hydrate and ensures that our revised CNT model is thermodynamically harmonious.

Keywords: heat transfer; mass transfer; methane hydrates; carbon dioxide storage; carbon dioxide hydrate; classical nucleation theory

Citation: Zarifi, M.; Kvamme, B.; Kuznetsova, T. Modeling Heat Transport in Systems of Hydrate-Filled Sediments Using Residual Thermodynamics and Classical Nucleation Theory. *Appl. Sci.* **2021**, *11*, 4124. https://doi.org/10.3390/app11094124

Academic Editor: Javier Rodríguez-Martín

Received: 3 March 2021
Accepted: 21 April 2021
Published: 30 April 2021

1. Introduction

Gas clathrate hydrate has long been a subject of many studies in the oil and gas-related industries, with hydrates as a flow hazard historically being both the focus and the main funding source for hydrate research. The basic building blocks of hydrates are hydrogen-bonded water cages which can trap molecules of certain non-polar substances. These encaged molecules (often referred to as "guest" species or hydrate formers) vary from light hydrocarbons such as methane and ethane, to acid gases such as carbon dioxide and hydrogen sulfide, and to compounds popular as refrigerants in the past. A great number of gas hydrate deposits exist both onshore and offshore all around the world, many of them considered viable potential sources of natural gas [1]. While the natural gas hydrates in sediments are rapidly becoming more and more relevant as an energy source, hydrate-related hydrocarbon fluxes into seawater and atmosphere poses a climate concern, with the geo-hazard aspects related to hydrate-filled sediments now coming to the forefront of hydrate research.

A fairly recent innovative approach to hydrate production calls for exchanging carbon dioxide for methane in natural gas hydrate reservoirs, providing a win–win scenario

of methane production combined with simultaneous safe CO_2 storage in the form of hydrate. This concept has often been envisaged as occurring at pressures needed for the CO_2 hydrate formation, which will be significantly lower than those of CH_4 hydrate at the same temperature. However, strictly speaking, those conditions are far from being relevant for practical implementations, since they are only relevant for the solid-state exchange mechanism, proven experimentally for temperatures far below zero by Kuhs et al. [2] and more recently Lee et al. [3]. Above the freezing point, hydrate deposits in the pores will always be in contact with free liquid water [4]. Even in Alaska permafrost, the average hydrate saturation amounts to only about 75%, with hydrate-filled sediment with saturation exceeding 80% being a very rare occurrence. These circumstances will give rise to a very fast mechanism for formation of new CO_2 hydrate from the injected CO_2. Heat released by this phase transition will be rapidly transported through the aqueous phases and assist in the dissociation of in situ CH_4 hydrate [3,5,6]. Since this is a liquid-state mechanism, its kinetic rates will be several orders of magnitude higher than those of a solid-state mechanism. Moreover, the two hydrate phases (in situ CH_4 hydrate and the newly formed CO_2 one) will not be actually in contact with each other, making the pressure–temperature equilibrium curves not particularly relevant for the purposes of analysis and illustration. The "exchange" phenomenon is rather a process of replacement, where a new hydrate fills the pore space originally filled with CH_4 hydrate.

The use of CO_2 for hydrate production is just one of many technologies currently considered for the purposes of releasing CH_4 from in situ hydrates while at the same time storing CO_2 in solid form as a hydrate. Regardless of the technology platform chosen, two criteria must be satisfied. The free energy change associated with the process has to be sufficient to dissociate the hydrate, and the necessary heat for hydrate melting must be supplied. Pressure reduction has long been the method of choice for dissociation of hydrates in natural gas hydrate reservoirs since it is easy to choose the production conditions lying outside hydrate stability limits based on the temperature–pressure stability curve of CH_4 hydrate. However, the question of the dissociation heat supply still remains. Limited temperature gradients will be established by the pressure reduction itself, as well as geothermal gradients. It is outside the focus of this work to discuss whether these gradients will be sufficient to sustain the melting process.

It would require far too much space to review all the various methods used in experiments and pilot–plant tests for CH_4 hydrate production. We have three decades of experience in experiments on CO_2/CH_4 exchange, and there is a plethora of literature already available on the topic. Similarly, there are numerous publications devoted to pressure reduction and studies of other methods. The focus in this work is mainly on the best way to model the phase transition thermodynamics and its associated kinetics. An important issue here is the need for a theoretically based model platform that accounts for all the implicit dynamic contributions to the phase transition. In order to accomplish this, we apply a fairly simple kinetic model based on theoretical considerations [7]. Yet, another important requirement to satisfy is a consistent thermodynamic model to describe the enthalpy changes taking place in hydrate phase transitions. With temperature, pressure, and concentrations as independent thermodynamic variables, Gibbs free energy will be the thermodynamic function determining phase stability. We need our models for enthalpy changes to be consistent with those for the Gibbs free energy.

Another area where hydrate phase transition dynamics become relevant is the transport of CO_2 in pipelines, which is a routine process in offshore Norway and many places around the world. Given the high pipeline pressures and low seafloor temperatures on the seafloor (typically below 6 °C), residual water present in the CO_2 stream may drop out either via condensation in bulk or adsorption on rusty pipeline walls and subsequently form a hydrate. Hydrate formation on small droplets liquid water will involve a dynamic balance between the driving force for hydrate formation (Gibbs free energy) and the transport of released heat through the insulating CO_2 fluid surrounding the forming hydrate core. Hydrate formation on liquid water films adsorbed on the rusty walls will also involve

the need to get rid of formation heat. While the liquid water and the pipeline wall will act as efficient heat conductors, pipeline insulation and the "bulk" CO_2 stream will hinder heat transport.

The examples presented above present just a few samples of practical scenarios involving implicit coupling between phase transition dynamics and heat transport dynamics. Theoretical physics provides a number of platforms suitable for modeling phase transition dynamics. Common to all of them is the implicit coupling between the mass transport dynamics characterizing the phase transition, the thermodynamics control (a function of Gibbs free energy change), and the heat transport.

The main focus of this work was to review some of the more recent and popular models applied to study hydrate phase transition dynamics in terms of actual kinetic rate limiting factors. Our secondary objective was to shed more light on the connection between nanoscale transition dynamics and hydrodynamic flow (which happens across a thin interface of 1–1.5 nm). Our third objective was related to the need for thermodynamic consistency. Many models describing enthalpy changes related to hydrate phase transitions are disconnected from the formal thermodynamic coupling between phase transition thermodynamics (Gibbs free energy changes) and the enthalpy changes related to heat transport requirements.

The paper is organized as follows. Section 2 provides an overview of popular models used to describe hydrate formation and dissociation dynamics in terms of characteristic transition properties. In Section 3, we outline a theoretical concept to serve as a basis for alternative kinetic models comprehensively accounting for implicit coupling between mass transport, heat transport, and thermodynamic control. It is important to point out here that the model we used is just an example chosen for illustration purposes. The need to include all the implicit dynamic contributions and to ensure thermodynamic consistency within the model are the important messages. Modeling results and associated discussion can be found in Section 4, while Section 5 provides the conclusions.

2. Literature Overview

Over the last several decades, a number of theoretical studies focusing on hydrate film formation along water/guest-fluid interfaces have been carried out by research groups worldwide [8–20]. The bulk of the studies considered either a planar gas–liquid interface, a water droplet surface in the gas phase, or the gas–bubble interface, with the theoretical research focusing on the impact of heat transfer on the growth of hydrates at the interface. As this paper aims to develop a more realistic kinetic model for hydrate film formation, we will mostly focus on the theoretical investigation by various researchers rather than experimental results.

The first theoretical models of hydrate film formation were developed by Shindo et al. [8], Lund et al. [9], and Teng et al. [10]; these studies can be broadly grouped together since their models describe the hydrate film as a diffuse layer suspended in the liquid hydrate former. Shindo et al. [8] treated each hydrate film as a concentration boundary layer, hypothesizing that water molecules will diffuse into the liquid CO_2 phase and subsequently give rise to hydrate nucleation, with the newly formed hydrate clusters slowly diffusing towards the aqueous phase. Lund et al. [9] extended the model by adding the possibility of hydrate cluster dissociating. Teng et al. [10] "reversed" the two models by presuming that hydrate will form more easily in the water–rich phase. However, all of the original three models have been shown to disagree with the experimental observations of a sharp solid–liquid interface and hydrate film tensile strength measurements by Sugaya et al. [11]

The second group of researchers utilized models that treated the hydrate film as a solid plate. For example, Hirai et al. 1996 [12] and Mori and Mochizuki 1997 [13] modeled the film as a CO_2-permeable micro-perforated plate model and a water-permeable micro-perforated plate, respectively. Unfortunately, the Hirai et al. [12] model failed to explain the driving force for the liquid CO_2 flow through the holes across the hydrate film, and

also used the unrealistic assumption of a mosaic water-side surface to explain the melting and crystallization of hydrates.

Later, Mori and Mochizuki 1997 [13] proposed a model similar to that of Hirai et al. [12] with respect to geometry and structure of the hydrate film. Their model assumes the hydrate film to be a uniform plate with constant thickness and evenly distributed micro–perforations. Their key difference in their description compared to Hirai et al. [12] was that it was the liquid water rather than the CO_2 that permeated the hydrate film and filled its capillaries. The process was driven by capillary pressure induced at the interface, with the aqueous phase inside the capillaries being saturated in guest species. The model assumed that CO_2 transfer into the aqueous phase and subsequent hydrate formation and dissociation processes will be rate controlled by mass transfer. A somewhat controversial point of this model was its assumption of hydrate melting and crystallization present even in the case of a vanishing driving force, as well as the lack of any consideration of kinetics governing the two processes. In 1998, Mori suggested a model describing the formation of hydrate film around a CO_2 droplet [14]. This new model was based on three new assumptions introduced to retard the dissolution of CO_2 in water. The first supposition involved the reduction in the droplet surface mobility due to hydrate film formation and the decrease in the convective mass transfer coefficient. The second assumption was the reduction in the solubility of CO_2 due to hydrate film formation, and the third one suggested that the effective viscosity of water and mass diffusion coefficient will increase because of hydrate cluster consumption of CO_2.

In 1999, Uchida et al. [15] experimentally observed hydrate film formation at the interface between water and CO_2. Their paper has also presented a theoretical analysis of the two-dimensional formation of a hydrate film, which is uniform in thickness and has a semicircular front. This model assumes that, firstly, the hydrate will only form at the film front where the temperature remains constant at the corresponding triple point (water/guest fluid/hydrate) value, and secondly, the rate of heat released by hydrate formation will be equal to the rate of heat removal by means of conduction through the film surfaces. Their study estimated the hydrate film thickness based on the lateral growth rate alongside the interface (still not fully reliable).

In 2001, Mori [16] extended their 1997 model by incorporating both heat and mass transfer involved in hydrate film formation and dissociation. Their steady-state (more accurately, quasi steady-state) one dimensional simulation of mass and heat transfer included the exothermic effect of hydrate formation and its inverse in the case of hydrate melting. They have also investigated the transient heat and mass transfer processes occurring during hydrate film formation, with their conclusion being that some mechanism other than heat transfer dominates the hydrate film formation, and heat transfer can be safely neglected when dealing with hydrate film thinner than 0.3 μm. In 2001, Freer et al. [17] applied a moving boundary model of heat transfer for the film hydrate formation to estimate the film thickness. They compared the obtained value with their own experimental result from a water/methane hydrate film and concluded that heat conduction was the dominant driving force. However, they denied the validity of their own conductive heat transfer model and proposed a model combining interfacial attachment kinetics via the Arrhenius expression and convective heat transfer instead.

In 2006, Mochizuki and Mori [18] carried out a numerical study of heat transfer across the water/hydrate-former phase boundaries. They applied two analytic models for methane and CO_2 hydrate film formation, derived by assuming two different film front geometries. Both models presumed a uniform film with constant thickness, with the thermodynamic triple point temperature set as the film front temperature. Their model assumed two-dimensional conductive heat transfer from the film front to hydrate formation sites and was able to predict the film formation rate if provided the film thickness. They estimated that a CO_2 hydrate film will be much thinner than a methane hydrate one at the same sub-cooling range. In addition, both CO_2 and methane films have exhibited a tendency to become thinner as the sub-cooling rate increased.

There is a need for a realistic kinetic model able to describe how the coupled processes of mass and heat transport will impact the formation and dissociation of hydrate, while accounting for all independent thermodynamic variables.

The bulk of available hydrate film formation studies fall into the hydrodynamic spatial range (micrometer and up), i.e., far beyond the scale of phase transitions itself. Phase transitions are nano-scale phenomena occurring across a thin interface only several nanometers in thickness. Many of the studies are based solely on estimates of film front propagation in terms of V_f and hydrate film thickness, while other papers also theoretically model the axial growth of hydrate films [19]. An obvious limitation of all models listed in Table 1 is that they account for heat transport only and ignore mass transport. This is an interesting and unusual assumption since heat transport through aqueous systems will be faster by a factor of two or three than mass transport [21,22]. The main assumptions of various models mentioned above include:

- Hydrate film having a homogeneous structure at the macroscopic level;
- Infinitely extending aqueous and guest-fluid phases and the interfaces between them;
- Spatially uniform hydrate film with thickness that does not vary with time;
- Hydrate crystal formation occurring only at the front of the hydrate film;
- The front temperature remaining constant at the three-phase equilibrium value;
- No advection occurring in either of the aqueous or guest-fluid phases.

Table 1. Properties needed for hydrate kinetic modeling, including details missing in hydrate phase transition models proposed by various research groups.

Hydrate Phase Transition Characteristics	1st Group [a]	2nd Group [b]	Mori and Mochizuki 1997, 1998	Uchida et al. 1999	Mori and Mochizuki 2001	Freer et al. (2001)	Mochizuki et al. (2006)	Mochizuki et al. (2017)	Liu et al. (2018)	This Work Model
Score [c]	1	1	1	1	1	1	2	3	3	4
Phase transition thermodynamic control	_ [d]	_	_	_	_	_	√ [d]	√	√	√
Phase transition mass transport kinetics	√	√	√	√	√	_	√	√	√	√
Phase transition heat transport kinetics	_	_	_	√	√	√	√	√	√	√
Irregular hydrate surfaces	_	_	_	_	_	_	_	_	_	_
Inhomogeneous (heterogeneous)hydrate	_	_	_	_	_	_	_	_	_	_
Hydrodynamic level mass flow	_	_	_	_	_	_	_	_	_	√
Hydrodynamic level heat flow										
Enthalpy changes	_	_	_	_	_	_	_	_	_	√
Changes in heat capacity	_	_	_	_	_	_	_	_	_	√
Changes in volume	_	_	_	_	_	_	_	_	_	√

[a]: Shindo et al. [8], Lund et al. [9], and Teng et al. [10], [b]: Hirai et al. 1996 [12] and Mori and Mochizuki 1997 [13]. [c] Scores are on a 0–5 scale based on the major aspects accounted for by each model; a model able to fully cover all the three aspects would be scored at 5. [d] (_) Hyphen indicates that the model in question ignores this aspect altogether; while (√) checkmark indicates that this aspect is accounted for, to a certain degree. The overall score reflects our opinion on the general comprehensiveness of the theoretical treatment as a whole.

Based on experimental observations of important dynamic features such as hydrate film thickness as a function of time and comparison to their previous studies, Mori and Mochizuki [19] have recently introduced two major interlinked assumptions:

- Spatial non-uniformity of temperature at the film edge;
- A variation in the guest concentration on the aqueous-phase side (i.e., mole fraction of water/hydrate at the two-phase equilibrium over the film front surface).

The most recent study in this overview, that of Liu et al. [20], considered natural convective heat transfer along with the gas–liquid interface. Unlike the previous studies, this model does contain a quantitative relation between the hydrate film formation and experimental temperature. Their model also proposes a sub-cooling correlation and an assumption that heat exchange between gas and aqueous phases will not influence the diffusion of hydrate film.

In Table 1 we briefly list certain basic physical quantities we believe to be essential for the kinetics of hydrate formation and dissociation. The three first rows describe the level of handling of the implicit coupling between mass transport, heat transport, and thermodynamic control of a given hydrate phase transition.

One can apply mass flux equation from the classical nucleation theory (CNT) to relate the two first hydrate transition properties of Table 1. The associated enthalpy change can be then directly coupled to the free energy change present in the thermodynamic control term via a trivial thermodynamic relationship. In more advanced theories, the coupling is slightly different and even more implicit. However, for screening purposes, even a complete description in accordance with the CNT would be scored as 5. Anything in between is based on a subjective evaluation. These first three elements are intimately related to the initial nucleation stage and are thus nanoscale in both space and time dimensions. The main purpose of the table was to provide a better basis for selection of models that have potential as platforms for further improvements. The fourth element contains both nanoscale aspects and higher level aspects. Several studies probing the phenomena at nano- to mesoscale have clearly demonstrated that nucleation is favored in inclinements or regions of restricted space between solid surfaces because molecules (both water and hydrate formers) become trapped there. Even if this trapping only lasts for a limited interval, the molecules will still take more time to rearrange into a hydrate as compared to a "bulk" or interfacial solution of hydrate formers in water. However, if the inclinements are too narrow, a destabilization of the hydrate core is more likely due to mechanical strain on a small hydrate nucleus squeezed in between solid surfaces.

A thermodynamically non-equilibrium situation will remove the chemical equilibrium constraint (equality of chemical potentials for all components in all the phases), leading to components with the highest affinity for water and the lowest volatility to be the best candidates to form hydrates first. In this study, we limit ourselves to components forming structure I and II hydrates. While the three first rows are directly related to the phase transition itself, the hydrodynamic conditions outside of the growing or decaying hydrates will provide either a reservoir or a sink for heat and mass, hence the need for rows 6 and 7.

The availability of either experimental data or models suitable for the estimation of heat that has to be transported to and from hydrates is the reason for the next two rows. The estimates for volume changes will be required for various purposes, including the application of the Clapeyron equation.

3. Methods

This work uses a fairly basic model to describe the kinetics of hydrates, the classical nucleation theory (CNT). There were two reasons for this. The first one is that this theory makes the various contributions to the phase transitions quite obvious, with their relative impact for the various phase transitions of interest easy to compare.

The second reason stems from the fact that the model's simplicity makes it easy to incorporate into software used for hydrate reservoir modeling and hydrate risk evaluation. Using a multiphase flow simulator to evaluation the risk of hydrate formation during the processing and transport of hydrate-forming fluids such as hydrocarbon, CO_2, and H_2S is a computationally expensive endeavor requiring a numerically simple model. It is, however, very important to stress that our CNT version is very different from the original one. The

mass transport term in the original CNT does not actually apply to mixtures and lacks any interface between the "old" and the "new" phases. As will be discussed later, we have harnessed the power of molecular dynamics simulations (MD) to sample the changes in diffusivities across the interface between liquid water and hydrate.

We apply the residual thermodynamics approach to calculate the free energy change of the phase transition (see Equation (2) below). At the hydrate stability limit, this free energy change will vanish (various solutions of Equation (2) are plotted in Figure 1) and must be negative enough for any scenario involving hydrate nucleation to overcome the interfacial free energy barrier. The use of residual thermodynamics for all phases ensures a transparent treatment of free energy variation, thus enabling a quantitative comparison of phase stabilities.

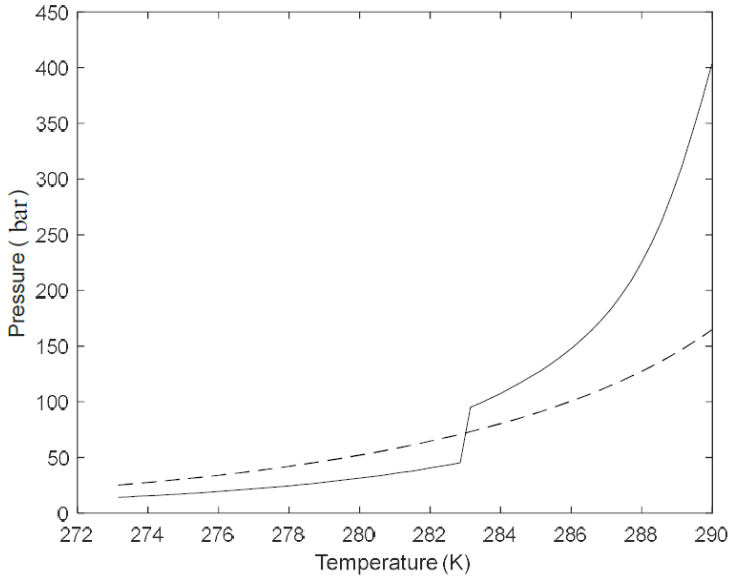

Figure 1. Hydrate stability region in the P-T projection of the stability regimes. The solid curve is for CO_2, and the dashed curve is for CH_4.

Energetic properties in classical thermodynamics are in principle only defined as differences and require a reference state for evaluation of total values. Residual thermodynamics utilizes pure-component ideal gas at relevant pressures and temperatures as the reference states, making the ideal gas mixing term is the first step towards the integration of any thermodynamic property of interest, which is simple enough in the case of energy Total energy or enthalpy of an ideal gas mixture is simply a proportional sum of pure component values. On the other hand, any entropic property must include an ideal gas mixing term related to the pressure variation from the pure component pressure to the partial pressure in the ideal gas mixture. The final stage is the integration from the ideal gas mixture to the real fluid mixture (gas, liquid, supercritical), usually performed using an equation of state [23]. In this work, the relevant properties containing ideal mixing changes are chemical potentials, free energy, and entropy.

A substantial advantage of utilizing ideal gas as a reference state is the direct linkage to classical molecular dynamics simulations (MD). In the classical limit, the momentum space (ideal gas) is orthonormal to the configurational space (residual properties). MD simulations sample the ideal gas properties from molecular velocities, rotational velocities, and velocities related to intramolecular movements, while the residual properties are estimated based on molecular interactions. The application of residual thermodynamics for hydrate and liquid water has been made possible via the modeling of the chemical potential of water in empty hydrate structures, ice, and liquid water [7]. This approach provides comparable free energies for all phases potentially co-existing in systems of hydrate formers and water. We also can obtain free energies of different hydrate phases

and thus compare their relative stability [21,24–28]. Given the limited space, the reader is directed to our earlier work on the fundamentals of CNT as applied to hydrates [29]. In this work, we mainly focus on heat release during the formation of hydrates.

Unlike many other models describing enthalpy changes associated with hydrate formation and melting, our residual thermodynamic model is directly related to the free energy changes as illustrated by Equation (1) below. The heat transport kinetics will be implicitly coupled to Equation (1), and a trivial application of statistical mechanics will prove that using Equation (1) for enthalpy will provide a consistent coupling between free energy and enthalpy changes. The residual, or configurational partition function, will be directly linked to the phase structure. Consistent descriptions of enthalpy and free energy will be needed in order to provide the correct entropy change for the phase transition; to the best of our knowledge, Equation (5) is the only enthalpy model in the available literature that satisfies this requirement.

Equation (1) below is a fundamental classical thermodynamics relationship; its derivation is available in any textbook and requires no further explanations.

$$\frac{\partial\left[\frac{\Delta G^{Total}}{RT}\right]_{P,\vec{N}}}{\partial T} = -\left[\frac{\Delta H^{Total}}{RT^2}\right] \tag{1}$$

where G is free energy and H is enthalpy. The Δ symbol is the change in free energy and enthalpy, respectively. The subscripts on the left brackets denote constant pressure and mol numbers. The free energy change related to the formation of hydrate on the interface between a separate hydrate former phase and liquid water can be expressed as

$$\Delta G^{(H)} = \begin{bmatrix} x^H_{H_2O}(\mu^H_{H_2O}(T,P,\vec{x}^H) - \mu^{water}_{H_2O}(T,P,\vec{x})) \\ +\sum_j x^H_j(\mu^H_j(T,P,\vec{x}^H) - \mu^{gas}_j(T,P,\vec{y}^{gas})) \end{bmatrix} \tag{2}$$

where μ denotes chemical potential. Subscripts H_2O and j denote water and hydrate formers, respectively. Superscripts H, water, and gas stand for hydrate, liquid water, and gas phases, respectively. x is the corresponding mole fraction in either the liquid or hydrate phase (superscript H), and y is the mol fraction in the hydrate former phase. T and P; are temperature and pressure. Due to the implicit and consistent coupling between free energy (a function that determines phase stability) and enthalpy, it makes sense to relate the changes in enthalpy to the phase stability boundaries. This connection is illustrated by the link between the pressure–temperature hydrate phase stability boundaries in Figure 1. The validity and accuracy of the calculations involved in the construction of Figure 1 have been verified through comparison with experimental data in many of our previous papers. For all the practical purposes, this means that the chemical potentials and free energies involved in Equation (2) have also been confirmed. Figure 1 is actually constructed so as to ensure that the free energy change given by Equation (2) is equal to zero.

In summary, the treatment of enthalpy changes in this work is entirely different from that used in many other enthalpy models. All our calculations are based on residual thermodynamics and the link through Equations (1) and (2). For this same reason, we do not refer to many publications from other research groups. There are certainly many high-quality publications dedicated to calculations of enthalpy changes in hydrate phase transitions. However, since they are based on very different thermodynamic platforms and reference systems, a review of these models would require too much space and will be of limited value for the main focus of this paper.

The liquid water chemical potential has been calculated using the symmetric excess conventions as described in Kvamme et al. [29] and Kvamme [30]. Equations (1) and (2) are coupled to an implicit equation for mass transport flux and thermodynamic control through Equation (22) in Kvamme et al. [29]. Superscript total in Equation (1) signifies the sum of Equation (2) and the penalty due to the work required to push aside the surrounding

phases to make room for the hydrate. This penalty term is proportional to the interfacial free energy (see Kvamme et al. [7] for more details).

The chemical potential for water in the hydrate structure is given by [5]

$$\mu^{H}_{H_2O} = \mu^{O,H}_{H_2O} - \sum_{k=1,2} RTv_k ln\left(1 + \sum_i h_{ij}\right) \quad (3)$$

in which superscript H denotes hydrate, with the superscript "0" in the first term on right-hand side referring to an empty clathrate lattice. These chemical potentials are readily available from model water (TIP4P) simulations of Kvamme and Tanaka [7]. The number of cavities per water ν_k is 1/23 for small cavities of structure I and 3/23 for large cavities. CO_2 is not able to provide significant stabilization of small cavities and has only been detected there at temperatures far below zero. The lack of liquid water interface under these ice conditions entails an entirely dissimilar hydrate formation mechanism where the gas side of the interface plays a different part. At temperatures above the freezing point and with CO_2 as the only guest, the sum over canonical partition functions for small and large cavities will include large cavities only:

$$h_{ij} = e^{-\beta[\mu_{ij} + \Delta gj]} \quad (4)$$

where β is the inverse of the universal gas constant times temperature. At equilibrium, the chemical potential of guest molecule j in hydrate cavities will be equal to its chemical potential in the co-existing phase it originated from.

3.1. Enthalpies of Phase Transitions from Residual Thermodynamics

A residual thermodynamics route to calculations of enthalpies of hydrate formation and dissociation has been recently proposed by Kvamme [30]. We refer the reader to that work for the details of all intermediate steps involved in the derivation of the right-hand side of Equation (3) using Equation (1), and only the final result is provided here:

$$H^{H}_{H_2O} = -RT^2 \frac{\partial\left[\frac{\mu^{0,H}_{H_2O}}{RT}\right]_{P,\vec{N}}}{\partial T} + \left[\sum_{k=1,2} v_k \frac{\sum_i h_{ki}\left[\left(H_{ki} - \Delta g_{ki} + T\frac{\partial \Delta g_{ki}}{\partial T}\right)\right]}{(1 + \sum_i h_{ki})}\right] \quad (5)$$

Enthalpies involved on the liquid water side of the phase transition can be trivially obtained by numerical differentiation of the polynomial fit of chemical potential as described in Kvamme and Tanaka [7], with the thermodynamic properties of the hydrate former phase and water in Equation (5) also being trivial to obtain. In the relevant temperature range of about 10 degrees (273 K–283 K), the differences in enthalpies as calculated from Equation (5) using Monte Carlo data do not vary substantially and can even be set as constant for the purposes of this work. This result is rather expected due to the hydrate water lattice being fairly rigid. The average motion of water atoms will mostly identical, while the sampled cavity partition functions will, of course, vary significantly over the same temperature range (see also the fitted functions of T in Kvamme and Tanaka [7]). The enthalpies of various guest molecules in the two types of cavities were evaluated by means of Monte Carlo simulations along the lines described in Kvamme and Lund [31] and Kvamme and Førrisdahl [32]. For a limited range of roughly 15 K from 273.15 and up, the residual energies remained virtually constant and amounted to −16.53 kJ/mol, −17.73 kJ/mol, and −27.65 kJ/mol for CH_4 in a large cavity, CH_4 in small cavity, and CO_2 in large cavity, respectively. The associated sampled volumes of movement/occupation were 164.2 Å^3, 89.21 Å^3, and 135.6 Å^3, respectively.

3.2. Heat Transport Related to Hydrate Phase Transitions

The two primary ways of heat transport relevant for the systems discussed in this work are conduction and convection. In the discussion that follows, we will consider systems where the initial amounts of water and CO_2 are large enough to not be consumed during the hydrate growth.

In the case of hydrate nucleation and growth inside a pipeline, the new mass will continuously be supplied by the flow stream. Offshore methane gas hydrates in sediments are typically characterized by methane coming from below through the fracture systems. A continuous inflow of water though fractures connected to the seafloor above will ensure a supply of liquid water but will also cause the hydrate to dissociate due to severe lack of dissolved methane. The chemical potential of CH_4 in the incoming water will therefore be close to its infinite dilution chemical potential, which is typically substantially lower than the chemical potential of CH_4 in hydrate. A typical sediment example in the case of CO_2 will involve aquifer storage of CO_2 in reservoirs that contain regions favorable for hydrate formation. Liquid water is available in the sediments, and a continuous inflow of CO_2 will lead to the formation of hydrate films that will reduce vertical CO_2 migration. In addition to the presence of natural sealing (clay, shale), these hydrate films reduce risk of CO_2 leakage to the surroundings above the storage site. These two practical examples alone illustrate the importance of having a model that assumes that the original "bulk" phases of the water and hydrate former phase will not be totally consumed and disappear. There are numerous other relevant examples.

A typical simplified heat transport model in our scenarios will involve heat conduction through the water over the growing film. The simplest approach would be a sum of symmetric heat conduction from below the hydrate growth site and heat conduction through the hydrate film towards the CO_2 phase. When the temperature on the hydrate surface reaches the hydrate melting point, an additional term of hydrate dissociation dynamics will enter the mass and energy balances. Additionally, mineral bedrock may also play a part in the overall energy balance, and it is entirely feasible to include the associated heat transport even within the framework of a very simple model. When the liquid water phase has been depleted in the CO_2 to the level of quasi-equilibrium with the CO_2 hydrate, a new hydrate can only form in one of the two ways: (1) CO_2 transport through the hydrate film and into the liquid water side of the hydrate film, or (2) water transport through the hydrate film and into the CO_2 side of the hydrate film.

The diffusion of CO_2 through hydrate will be very slow and most probably limited by the existence of empty cavities; this process will trigger the temporary local destabilization of the water hydrate lattice and induce a counter diffusion of water molecules.

In the absence of "fresh" building blocks, the first and second laws of thermodynamics will lead to a dynamic process in which the least stable hydrates (those with highest free energy) are undergoing melting to support the growth of hydrate regions with lower free energy [29]. Even by themselves, these processes can generate mass fluxes across the hydrate membrane film. Ultimately, these local free energy-governed processes can even lead to the creation of holes in the hydrate membrane, allowing for the supply of new building blocks.

A common approximation in hydrate modeling, as well as in the interpretation of experimental data, is, therefore, to lump both these contributions together into an apparent conductivity:

$$\dot{Q} = K\frac{V^{film}}{A_{\perp}}\Delta T \tag{6}$$

where $A_{\perp}$ is area normal to the heat transport direction, and V^{film} is the volume of hydrate film.

Heat transport through liquid water and hydrate will be very fast, and two to three orders of magnitude faster than mass transport [21,22]. Work is in progress on a more detailed review of available theoretical estimates of diffusion through hydrate. The available values range from 10^{-15} m^2/s to 10^{-17} m^2/s for diffusivity of CH_4 through hydrate, with

the corresponding CO_2 values likely to be slightly lower. However, the huge variation illustrates the existing uncertainty in the correct way to handle this transport, with the bulk of the studies based on some sort of cavity-jumping Monte Carlo calculations. This is basically a mathematical–statistical method, and other types of approaches might be required. One hypothesis suggests that the more vigorous process of water librations in empty cavities facilitates a temporary destabilization of the water lattice due to the motion of guest molecules in the neighboring cavities. This may eventually allow the guest molecules to enter into the previously empty cavity. This hypothesis is based on the observation of Kvamme and Tanaka [7] and how various guest molecules interfere with water lattice librations. Regardless of the mechanism, these phenomena will result in increased diffusion, with the mass transport through a hydrate film accordingly expected to be proportional to the square root of time with a constant rate. The first part of a film growth model is simply the time a guest molecule will need to travel across the hydrate film. The resulting heat of the hydrate formation will be distributed locally as heat transport through liquid (Kw) and through hydrate (K_H) up to the hydrate dissociation temperature. The remaining fraction of the released heat will lead to the local partial dissociation of the hydrate film.

The curves characterizing heterogeneous (water and a separate hydrate former phase) hydrate dissociation or hydrate formation will be given by the temperature–pressure projection of hydrate stability conditions, see Figure 1 for examples in the case of CH_4 and CO_2. See Kvamme [24] and Kvamme and Aromada [25] for verification of the model behind Figure 1 through comparisons with experimental data. As mentioned before, the plotted curves are the solutions of Equation (2) when the free energy change is set to zero. The chemical potential for water in hydrate is calculated from Equation (3) using guest partition functions from Equation (4). The estimation of the liquid water chemical potential utilized the pure liquid water chemical potential from Kvamme and Tanaka [7], with activity correction added in the case of additives such as alcohols or ions present. Setting the chemical potentials of the hydrate former in the hydrate equal to its value in the separate hydrate former phase will allow one to solve Equation (2) by means of iterations.

Additionally, note a very sharp increase in the hydrate stability curve in the case of CO_2 due to its phase transition from gas to liquid with a significantly higher density and a corresponding shift in thermodynamic properties. This changeover is frequently ignored in the published hydrate equilibrium data, with artificial smoothening of the CO_2 hydrate equilibrium curve creating a bias in quite a number of published datasets.

A simple model describing the dynamic progress of the system following the hydrate former reaching the liquid water side will be given by

$$\left(dJ_{formation}A_{H_{formation}}\Delta H^{formation}(T,P)\right) = K_w\Delta T_w dR_w + K_H\Delta T_H dR_H + K_m\Delta T_m dR_m + dJ_{dissociation}A_{H_\alpha}\Delta H_\alpha^{dissociation}(T_\alpha,P) \quad (7)$$

The "*formation*" superscript over the delta *H* denotes the enthalpy change of hydrate formation associated with the guest molecules entering the liquid water side. The simplest scenario will be represented by an evenly distributed growth flux across a planar surface of initial hydrate film. R is the distance of heat transport. Subscript w denotes liquid water, subscript H stands for hydrate film, and m indicates minerals. In the case of liquid water and hydrate, the reference temperature is that of hydrate formation; it is approximated by the average of the surface area normal to the mean mass flux through the sediment in the case of minerals.

For the hydrate film, the heating contribution (the second term) will continue to increase up to the hydrate dissociation point corresponding to the actual pressure (see Figure 1). After that, heat transported in this direction will be split between the dissociation of hydrate and raising the hydrate temperature.

As can be seen from Table 2 below and the associated discussion, the reported experimental values of heat conductivity through hydrate vary significantly. The difference in

liquid water heat conductivity is, however, limited. If the K-values for hydrate and liquid water are assumed to be identical, then the temperature difference from one time step to the next will be the same whether the conduction is through liquid water or hydrate. To simplify conductivity for both the hydrate and water phase, they are the same up to two limits. The first limit is when hydrate dissociation begins; another limit is if the heat transport through the hydrate approaches the hydrate former phase, which is almost heat insulating.

If we ignore the mineral surfaces for a moment, Equation (7) can be rewritten into the following one-dimensional form:

$$\left(dJ_{formation} A_{\perp} \Delta H^{formation}(T,P)\right) = K\Delta T_w d\vec{R} + K\Delta T_H d\vec{R} + dJ_{dissociation} A_{\perp} \Delta H_{\alpha}^{dissociation}(T_{\alpha},P) \quad (8)$$

The purpose of vectorial R is only to indicate the direction relative to a reference point. With the reference point set so that $R = 0$ at the hydrate surface, the hydrate former entering the aqueous phase will correspond to positive R, while transport through the hydrate film will be indicated by negative R values. The second reasoning behind the vector notation in the context of (8) is to ensure absolute values for both the first and the second terms. Both the left-hand side and the third term on the right-hand side, are also absolute values, allowing Equation (8) to describe the distribution of heat released during hydrate formation.

While Equation (8) is clearly oversimplified, there is some justification for it for the systems in consideration. Heat transport through liquids is normally two to three orders of magnitudes faster than mass transport [21–29], which also explains the difference in flux rather than associated heat release (or consumption). Transporting the guest molecules through a hydrate film from the gas side to the liquid side to sustain the growth may be 8 to 10 orders of magnitudes slower than diffusion of the same molecules though liquid water. As such, it will be fairly safe to assume that any guest molecules that reach the liquid water side will instantly dispose the hydrate formation heat due to the combination of the three terms in Equation (8).

A number of theoretical methods for estimating thermal conductivity are available in the literature as well as substantial amounts of experimental data from different research groups worldwide. It is far outside the focus of this work to conduct a detailed review of theoretical models and experimental data for thermal conductivities of relevance to this work. As such, the literature values in Table 2 are listed with reference to the actual sources without any additional comment.

Generally, gas hydrates exhibit a glass-like behavior where it comes to the temperature and pressure dependence of their thermal conductivity. This feature makes them drastically different in comparison to ice and other molecular crystals [33]. In hydrates, the water framework is much more distorted, with the hydrogen bond more strained than in ice. This results in the inhibition of long-range modes and spatial localization of energy, suggesting that their low thermal conductivity is not only due to guest–host interactions. The rigidity of the framework and hydrate lattice structures will also contribute lower thermal conductivity of clathrates compared to ice. Both available models and experimental data point to a typical hydrate thermal conductivity of 0.45–0.7 W/(m·K) within the temperature range 265 K to 280 K. Taking methane hydrate as an example, thermal conductivity measured in compacted samples using a needle probe at conditions similar to those in natural environments amounted to 0.62 ± 0.02 W/(m·K) [33]. The only reported value for the CO_2 hydrate thermal conductivity is 0.49 W/(m·K) [34].

Table 2. Thermal conductivity of different hydrate components in various phases.

Material	Thermal Conductivity (Experimental Values) W/(m·K) [1]
	Aquas Phase
Liquid Water (273 K–283 K)	0.56–0.58
Sea Water	0.56–0.57 [35]
CH_4 (liq)	[36]
CO_2 (liq)	[37]
	Gas Phase
CH_4 (gas)	0.0297 (260 K, 1 MPa) 0.035(at 4.98 MPa, 277 K)
CO_2 (gas)	0.093512 [37]
	Minerals
Quartz	6.6–8.4 [38]
Calcite	3–4.5 [38]
Kaolinite	1.8–3 [38]
	Hydrate Phase
CH_4 Hydrate	0.57 (263 K) [33] 0.62 [32] 0.68 (261.5–277.4) [33]
CO_2 Hydrate	0.49 [34]

[1] Thermal conductivity: W/ (m·K) = 2.390 × 10^{-3} cal/cm sec °C = 0.5797 Btu/ft hr °F.

In view of the above, Equation (8) has been reformulated in terms of the mass transport across the hydrate/liquid water interface during the hydrate formation:

$$A_{\perp}\left(\frac{dJ_{formation}}{d\vec{R}}\right)\Delta H^{formation}(T,P) = K\Delta T_w + K\Delta T_H + A_{\perp}\left(\frac{dJ_{dissociation}}{d\vec{R}}\right)\Delta H_{\alpha}^{dissociation}(T_{\alpha},P) \quad (9)$$

The diffusivity across the interface from the liquid water side (R = 0 Å) to the hydrate side of the interface (R = 12 Å) is not known and is difficult to model using Molecular Dynamics simulations or other approaches. The profile in Figure 2 is, therefore, to be considered empirical, although it contains some interpretations of water movements during the dissociation of hydrates. It is considered sufficient for the purposes of this work.

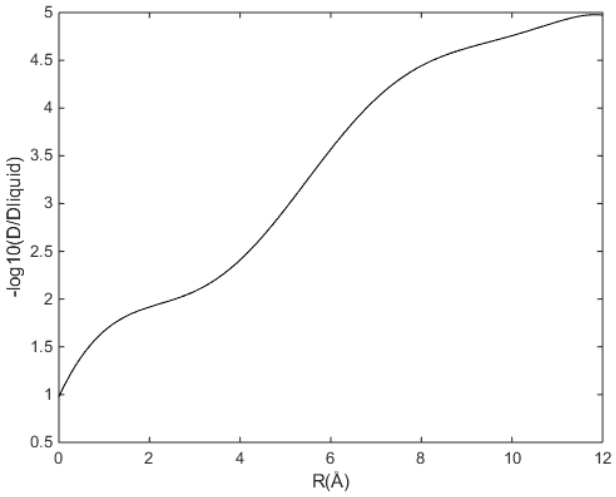

Figure 2. Relative diffusivities of CO_2 across the interface from liquid water side to hydrate interface side.

A mathematical fit to the profile in Figure 2 is

$$-\log_{10}\left[\frac{D(R)_j}{D_{liquid,j}}\right] = \sum_{i=1}^{9} a_i\left(a\tan\left[\left(0.5R\frac{\pi}{2}\right)/12\right]\right)^{i-1} \quad (10)$$

j = CO_2, CH_4, with parameters given in Table 3.

Table 3. Parameters for Equation (10).

i	Parameter	I	Parameter	i	Parameter
1	0.979242	4	171.673	7	−9649.96
2	15.5427	5	6.76975	8	14,779.7
3	−88.5112	6	1939.55	9	−7496.15

However, in the context of this work, the most important aspect is to shed more light on the relative importance of various contributions to the implicitly coupled mass and heat transport dynamics related to hydrate phase transitions.

Fick's law will give:

$$J(R) = \left[-D_{CO_2}(R)\frac{\partial C(R)}{\partial R}\right] \tag{11}$$

while the derivative of mass flux across the interface can be written as

$$\frac{dJ(R)}{dR} = \left[-\left(\frac{dD_{CO_2}(R)}{dR}\right)\left(\frac{\partial C(R)}{\partial R}\right) - D_{CO_2}(R)\frac{\partial C^2(R)}{\partial R^2}\right] \tag{12}$$

The appropriately derived concentration profile of CO_2 across the water interface is illustrated in Figure 3 below:

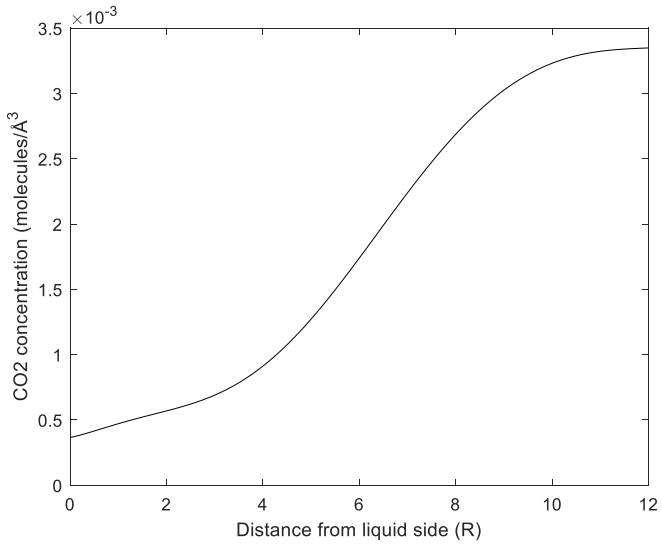

Figure 3. Concentration profile for CO_2 across water (R = 0)/hydrate (R = 12) interface [39–41].

4. Results and Discussion

The stability of a hydrate phase will ultimately depend on all independent thermodynamic variables of the systems. These include temperature, pressure, and concentrations of the components in all of the co-existing phases. It is possible to plot various projections of hydrate stability onto a sub-set of independent thermodynamic variables, with temperature and pressure projections being the most typical example, as illustrated by stability the limits of CH_4 and CO_2 hydrates in Figure 1. As noted previously, the phase transition undergone by CO_2 will significantly affect the temperature-pressure projection of its hydrate existence region. Given that temperatures and pressures are independent thermodynamic variables, it is the hydrated Gibbs free energy that will determine the phase stability. The free energies of hydrates formed along the corresponding hydrate stability limits of Figure 1 are plotted in Figure 4. CO_2 will form a more stable hydrate

than CH_4 for the whole range of thermodynamic conditions covered in Figure 1. In order to illustrate impact of a typical hydrate inhibitor, we also present the curves of Gibbs free energy for hydrate formation from the aqueous phase containing various mole fractions of methanol. The more methanol is added, the less stable the formed hydrate will be.

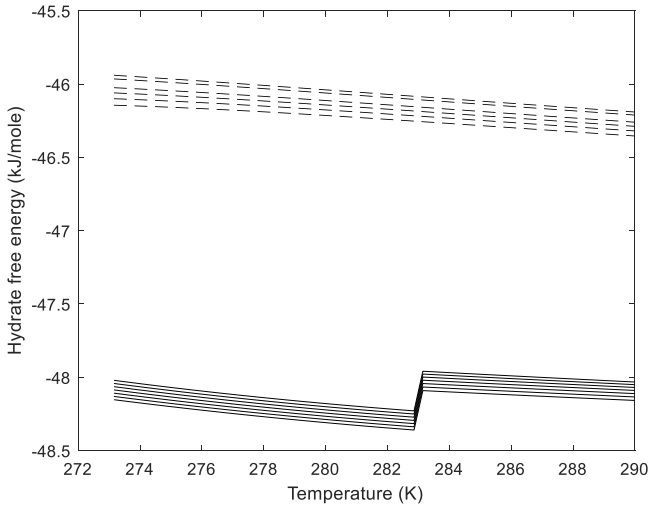

Figure 4. Calculated free energies of CO_2 hydrates (solid) and CH_4 hydrates (dashed). For each set of curves, the lowest curve is the free energy of hydrate formed from pure water, with the curves above corresponding to the following methanol content: 2 mol %, 4 mol %, 6 mol %, 8 mol %, 10 mol %, and finally 12 mol % for the topmost curves of CO_2 and CH_4, respectively.

Since Figure 5 may not be easily interpreted, the understanding of its plots should benefit from an additional reading of the two related 2D figures. Figure 5 shows the co-variation of pressure and temperature, while Figure 6 below shows enthalpy changes along the temperature projection of Figure 1.

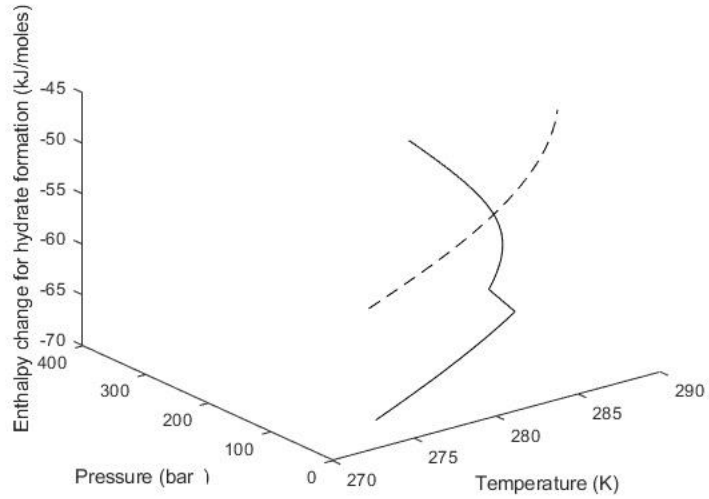

Figure 5. Enthalpy changes associated with hydrate formation along the hydrate P-T equilibrium curves for CO_2 hydrate (solid) and CH_4 hydrate (dashed). Units are kJ/mol hydrate former.

What is even more important in the context of this work are the differences in enthalpies of hydrate formation along the hydrate formation curves presented in Figure 6. One of the reasons for presenting the data for varying concentrations of methanol in the aqueous phase in Figure 4 is the fact that methanol also will act as a surfactant where the water/hydrate-former phase is concerned. This can be used to stimulate the CO_2/CH_4

exchange process since the methanol-enriched interface will hinder the formation of a sealing hydrate film between water and hydrate-former phases.

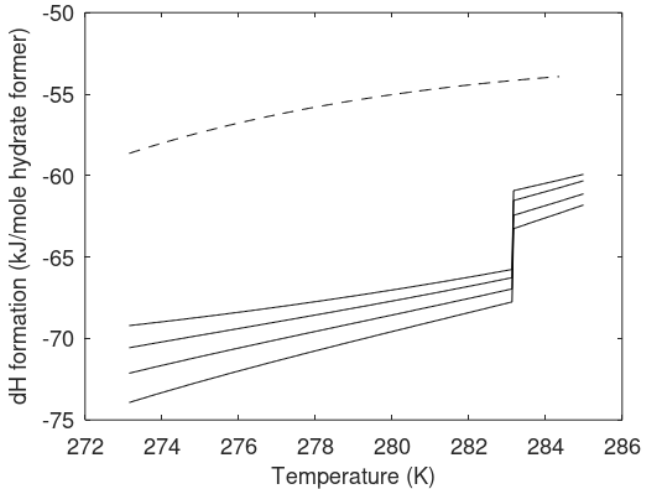

Figure 6. Enthalpies of hydrate formation in kJ/mol hydrate former as function of temperature. For temperatures below the CO_2 phase transition point (roughly 283.4 K), the bottom solid curve corresponds to CO_2/CH_4 mixture with 10 mol % CH_4; the top solid curve is pure CO_2; 5 mol % CH_4 and 2 mol % CH_4 curves fall in between. For temperatures above the CO_2 phase transition point, the order of curves is reversed. The dashed curve is the corresponding results for pure CH_4 hydrate.

In accordance with Figure 5, the heat of hydrate formation will be about 10 kJ per mol of hydrate former larger for the CO_2 hydrate compared to methane hydrate. Heat released when new CO_2 hydrate is created from the injected mixture of CO_2 and surfactant will be transported through the aqueous phase in front of the CO_2 plume. A portion of heat will be lost to the heating of the bedrock; an increased concentration of ions due to pore water being consumed by the forming CO_2 hydrate is another important side effect of this process. The latter phenomenon is where Figure 5 comes into play more directly, since CH_4 will dissolve more vigorously when the ion activity goes up.

The injection of CO_2 into CH_4 hydrate-filled sediments will lead to the formation of new CO_2 hydrate from injected CO_2 and free pore water. It is rare to find hydrates with a hydrate saturation exceeding 85% of the pore volume, with 75% or less hydrate filling being more common. The primary mechanism for dissociation of in situ CH_4 hydrate will be driven by the latent heat of the CO_2 hydrate formation. In a general case, it is safe to assume that CH_4 released by the dissociating methane hydrate will migrate away from the CO_2 hydrate, whose surface will contain hydrate films separating the fluid CO_2 from the released CH_4. In the case where we can expect a degree of mixing between the released CH_4 and CO_2, it will be instructive to examine how this will affect the enthalpies of formation. For ease of implementation, we will use 2D plots of hydrate formation enthalpies evaluated along the hydrate formation pressure limits. These plots should still yield fairly relevant conclusions for hydrate formation enthalpies since any Poynting pressure corrections within the hydrate stability region will be very small. Figure 6 will therefore present the enthalpies for pure CH_4 hydrate, pure CO_2 hydrate, as well CO_2/CH_4 mixtures with 98 mol % CO_2, 95 mol % CO_2, and 90 mol % CO_2 plotted as functions of temperature along with the corresponding temperature–pressure stability limits. A similar plot in Figure 7 shows the enthalpies of hydrate formation as functions of pressure along the temperature-pressure stability limits. Since a CO_2 molecule is too large to provide any stabilization of small cavities, 25% of small cavities will be empty for these ranges of conditions in the case of a pure CO_2 hydrate. As can be seen from Figures 6 and 7 below, the addition of CH_4 will therefore result in larger (negative) values for enthalpies of hydrate formation.

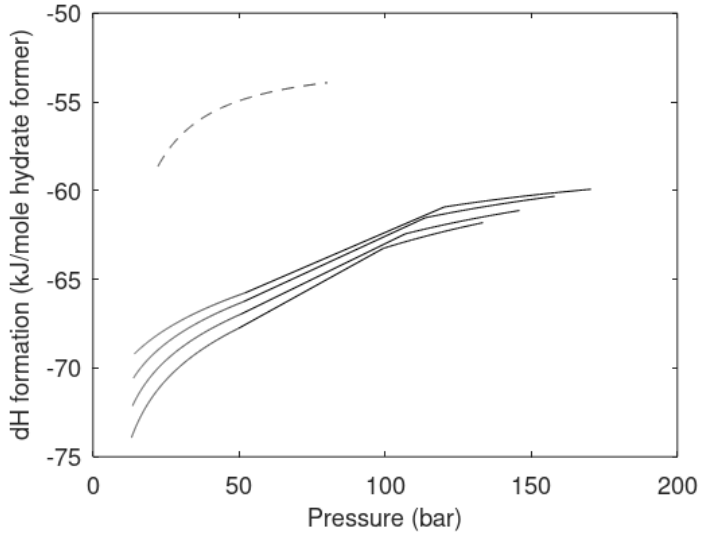

Figure 7. Enthalpies of hydrate formation in kJ/mol hydrate former as function of pressure. The bottom solid curve corresponds to CO_2/CH_4 mixture with 10 mol % CH_4; the top solid curve is pure CO_2; 5 mol % CH_4 and 2 mol % CH_4 curves fall in between. The dashed curve is the corresponding results for pure CH_4 hydrate.

The results presented in Figures 6 and 7 will also be relevant when the injected CO_2 comes from a separation plant used for removal of sour gases from hydrocarbons. As an example, millions of tons of CO_2 from the Sleipner field are separated and injected into the Utsira formation. The injection gas contains approximately 5 mol % of CH_4 [42].

In Figures 8 and 9, we plot the enthalpies of hydrate formation as a function of temperature and pressure along the hydrate stability limit curve.

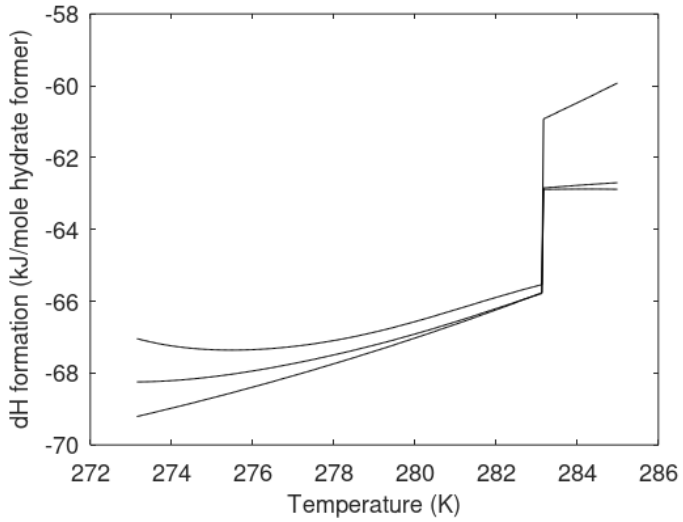

Figure 8. Enthalpies of hydrate formation in kJ/mol hydrate former as function of temperature. For temperatures below the CO_2 phase transition (around 283.5 K), the bottom solid curve corresponds to pure CO_2 hydrate; the top solid curve is 20 mol % N_2 in CO_2/N_2 mix; the middle curve is 10 mol % N_2 in CO_2/N_2 mix. Above the CO_2 phase transition, the order of the curves is reversed.

The use of pure component values for the enthalpies of hydrate formation will substantially simplify the modeling, with the motivation for including Figures 6–9 being to facilitate a qualitative picture of the sensitivity of hydrate formation enthalpies with respect to certain relevant additives. Other uncertainties taken into account, using pure component

values for modeling will provide a fair approximation only for temperatures below and fairly close to the CO_2 phase transition temperature, as illustrated in Figures 6–9.

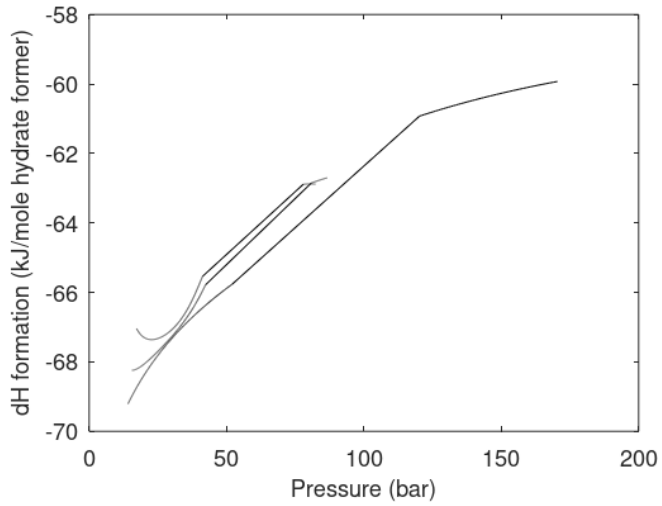

Figure 9. Enthalpies of hydrate formation in kJ/mol hydrate former as function of pressure. The bottom solid curve is pure CO_2 hydrate; the middle one is 10 mol % N_2 in the CO_2/N_2 mix; the top solid curve is for 20 mol % N_2.

As noted previously, heat transport in aqueous systems is faster than mass transport by an order of two or three, which is a well-known fact verified by several of our earlier publications on hydrate phase transitions [21,22]. It is therefore disappointing that so many kinetic theories are based on heat transport models rather than the associated mass transport limitations.

The following profile (Figure 10) is based on data obtained from the molecular modeling of interfaces typical for CH_4 and CO_2 hydrates [39–41]. Recently, a number of experimental studies have studied the use of CO_2 with limited admixture of N_2 intended to both avoid the blocking of pores by newly formed CO_2 hydrate and to increase the flow permeability of the injection gas at the same time (see for instance Kvamme [24], Kvamme et al. [43], and B. Kvamme [44]).

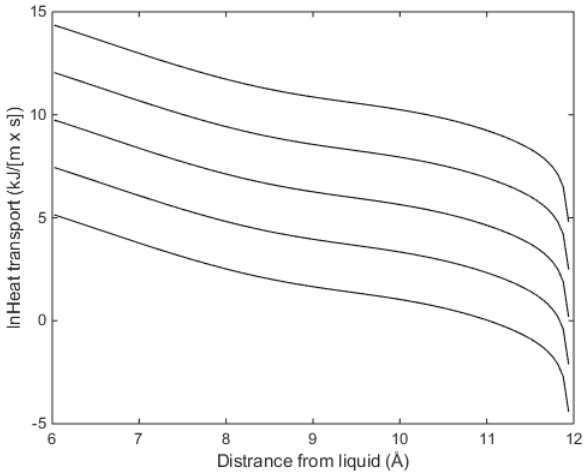

Figure 10. Calculated heat transport rates through hydrate/liquid water interface as a function of liquid-side diffusivity coefficient in Equation (10). Upper curve is for D liquid in Equation (10) equal to 1×10^{-07} m^2/s (top), 1×10^{-08} m^2/s, 1×10^{-09} m^2/s, 1×10^{-10} m^2/s, 1×10^{-11} m^2/s (bottom). Absolute minimum heat transport rate is 1.4×10^{-10} kJ/(m × s), 1.4×10^{-11} kJ/(m × s), 1.4×10^{-12} kJ/(m × s), 1.4×10^{-13} kJ/(m × s), and 1.4×10^{-14} kJ/(m × s) for the same curves.

As illustrated in Figure 5, the heat of hydrate formation enthalpy varies along the hydrate stability limit. At 273.16 K and 14.19 bars, the calculated value amounted to −67.8 kJ/mol CO_2, with the corresponding value at 290 K and 403 bars equal to −58.5 kJ/mol CO_2. Inserting the former value as the enthalpy of hydrate formation in Equation (9), and the profiles in Figures 2 and 3 in Equation (12), one can find the limiting heat transport rate. These calculations are illustrated in Figure 10 below for five different values of diffusivity on the liquid side of the interface (in Equation (10)) for the most rate limiting portions of the interface.

Heat cannot be transported faster than it moves across the rate-limiting sections, with many dynamic changes related to the mass and heat transport drastically changing the mass and heat transport rates. As an example, the calculated heat transport rates corresponding to the distance of 6 Å from the liquid side would be four orders of magnitude higher than the values used Figure 10. On the other hand, the heat conduction coefficient of 0.57 W/(m·K) (see Table 2), i.e., 5.7×10^{-4} kJ/(m·s·K), will still translate into heat transfer orders of magnitude faster than the mass transport-controlled rates on the left-hand side of Equation (9).

The heat transport models along the lines presented here can be incorporated into simple kinetic models such as the classical nucleation theory (CNT) for use in hydrate phase transition modeling at the pore level in reservoir simulation. Yet, other applications are kinetic extensions of our hydrate risk evaluation models (see, for instance, [24,25]).

In this work, we have shown that mass transport through hydrate/liquid water interface is very slow. This issue is likely to limit hydrate film growth, and this may interfere the balance between distribution of released heat and temperature increase in surroundings. This may lead to partial re-dissociation of the hydrate film. As an illustration of the slow transport through hydrate films, we will utilize a simple version of CNT for spherical hydrate cores. CNT can be formulated as

$$J = J_0 e^{-\beta \Delta G^{Total}} \tag{13}$$

where J_0 is the mass transport flux supplying the hydrate growth. For the phase transition in Equation (1), it will be a supply of CO_2 across an interface of gradually more structured water towards the hydrate core, as discussed in Kvamme et al. [29] and illustrated above (see Figures 2 and 3). The units of J_0 will be mol/m^2s for heterogeneous hydrate formation on the growing surface area of the hydrate crystal. β is the inverse of the gas constant times temperature, and ΔG^{Total} is the molar free energy change of the phase transition. This molar free energy contains two contributions: the phase transition free energy as described by Equation (1), and the penalty work incurred by pushing aside the old phases. Since the molar densities of liquid water and hydrate are reasonably close, it would be a fair approximation to obtain it as a product of molar free energy of the phase transition times the molar density of the hydrate times the volume of the hydrate core. The push work penalty term is simply given by the interface free energy times the surface area of the hydrate crystal. Using the underscore symbol to indicate extensive properties (in Joule):

$$\underline{\Delta G}^{Total} = \underline{\Delta G}^{Phasetransition} + \underline{\Delta G}^{Pushwork} \tag{14}$$

For the simplest possible geometry of a crystal, a sphere with radius R, we will obtain

$$\underline{\Delta G}^{Total} = \frac{4}{3}\pi R^3 \rho_N^H \Delta G^{Phasetransition} + 4\pi R^2 \gamma \tag{15}$$

where ρ_N^H is the hydrate molar density, and γ is the interfacial free energy between hydrate and the surrounding phase. Even if the hydrate core is floating on the water surface, one would expect small crystals to be covered by water on the gas side as well due to capillary forces facilitating the transport of water molecules from the liquid water side.

Differentiating Equation (15) with respect to R and solving for the maximum free energy radius (the critical core size) yields the usual result:

$$R^* = -\frac{2\gamma}{\rho_N^H \Delta G^{Phasetransition}} \tag{16}$$

where superscript * denotes critical nucleus radius. The critical radius for two different temperatures is given in Figure 11 below. For the temperature below the transition to liquid CO_2, the trend is very similar to that observed in Phase Field Theory (PFT) modeling (see [39–42] and the references therein).

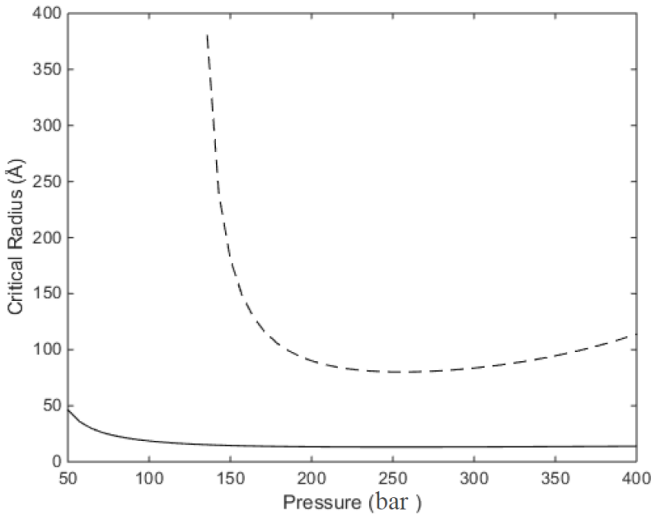

Figure 11. Calculated critical radius for heterogeneous nucleation of hydrate from CO_2 and liquid water as a function of pressure for 280 K (solid) and 285 K (dashed).

The transition into the liquid phase will dramatically increase the critical radius, although it will still remain at the nanoscale, except for the lowest pressures. Figure 12 presents nucleation times corresponding to heterogeneous hydrate formation from CO_2 and water phase at 280 K and 285 K, with the nucleation time above the carbon dioxide transition point much higher at lower pressures.

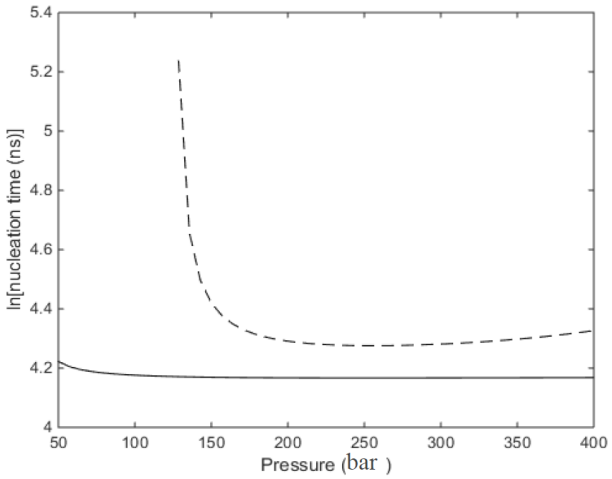

Figure 12. Calculated nucleation times for heterogeneous hydrate formation from CO_2 and liquid water. Solid curve is for 280 K, and dashed curve is for 285 K.

As noted earlier, diffusion through the initial hydrate film will be very slow. Since most estimates available in the literature are based on molecular modeling simulations

using specific approximations and assumptions, at least 12 different values can be found in journal papers; they range between 10 and 15 m^2/s and 10–17 m^2/s. As long a hydrate is formed, it will be the lowest free energy phase for water. The hydrate will therefore decide the minimum level of CO_2 in the contacting aqueous phase. This means that hydrates can grow from CO_2 dissolved in water from its solubility limit and down to the CO_2 hydrate stability limit (see Kvamme et al. [29] for more details).

Hydrate formation from the aqueous phase side will preferentially occur towards the already established hydrate film due to the presence of adsorbed and structured water in contact with the hydrate surface. However, the supply of hydrate former needed to sustain the growth will still occur via diffusion. Assuming a quasi-equilibrium between liquid water and water adsorbed on the hydrate surface, one can obtain a fair estimate of hydrate nucleation rate from CO_2 dissolved in water. Figure 13 presents the critical radius calculated for homogeneous hydrate formation from CO_2 dissolved in water for 280 K and 100 bars as an example. The corresponding nucleation times are plotted in Figure 14. We should note that this route to hydrate formation is characterized by almost "instant" hydrate nucleation in the macroscopic sense (nucleation time of mere seconds).

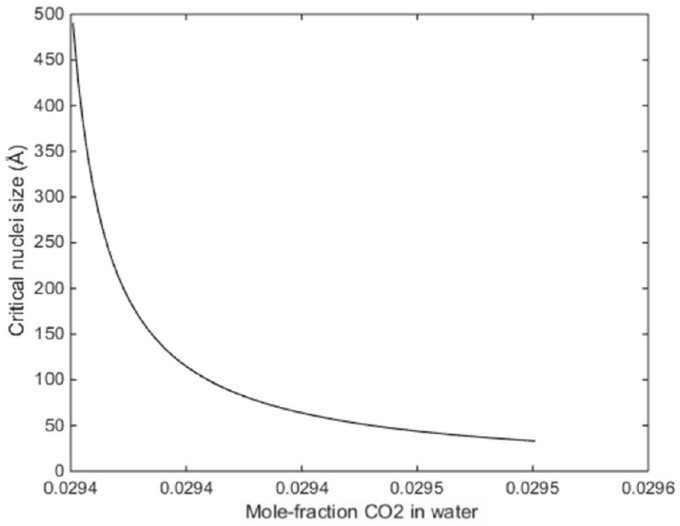

Figure 13. Calculated critical radius in the case of homogeneous hydrate formation from liquid water and dissolved CO_2 at 280 K and 100 bars as function of mole fraction of CO_2 in liquid water.

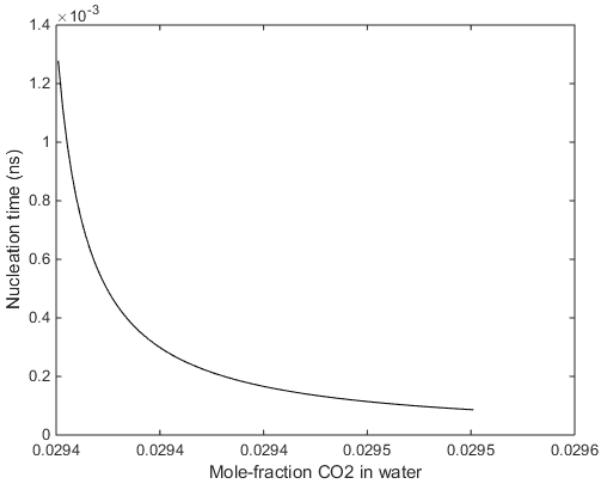

Figure 14. Calculated nucleation times in nanoseconds in the case of homogeneous hydrate formation from liquid water and CO_2 dissolved in water at 280 K and 100 bars.

Figure 15 presents the growth rates calculated by using the value of $D_{liq} = 10^{-08}$ m^2/s in Equation (10). The time for visible hydrate film appears to be in a good agreement with the observations of Uchida et al. [10], as well as our own observations of CH_4 hydrate film growth [40] that showed visible (Magnetic Resonance Imaging) hydrate on a resolution scale of approximately 300 microns after 100 h.

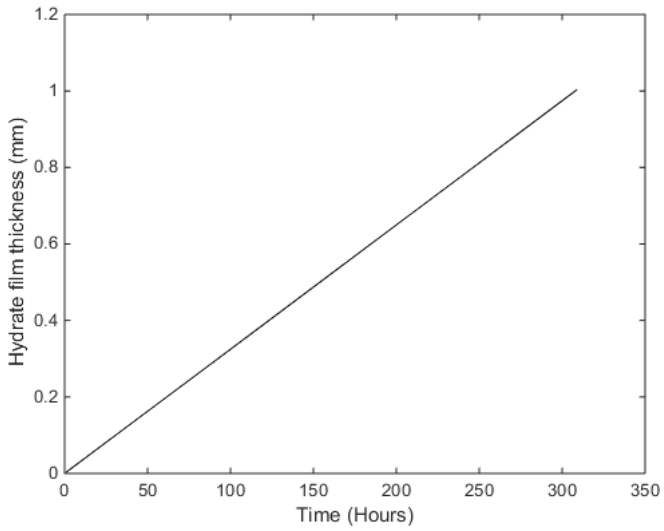

Figure 15. Calculated CO_2 hydrate film thickness as a function of time for a liquid side diffusivity in Equation (10) equal to $D_{liq} = 10^{-08}$ m^2/s.

It is beyond the scope of this work to provide a more detailed analysis of the induction times for various sets of transport characteristics and thermodynamic conditions. However, the results presented in this work will be applied in our modeling of hydrate dynamics in sediments, as well as in the dynamics of hydrate nucleation during pipeline transport of hydrate formers containing dissolved water.

MDIT (multicomponent diffuse interface theory) theory [45] is equally a simple and convenient alternative for practical applications that require quickly solved kinetic models. The heat transport modeling in this work will also find its way into our present level of Phase Field Theory (PFT) models. See, for instance, [24–26,38–40] for representative examples.

While the heat transport across aqueous systems is very fast, the opposite is true for hydrate formation from water dissolved in gas even though this process is thermodynamically feasible. Mass transport is slow since about 150 water molecules must assemble and structure themselves into a hydrate nucleus for it to be able to grow steadily. In this case, heat transport will be the rate limiting factor since the enthalpy of creating the hydrate core needs to be transported through a heat insulator such as hydrocarbon gas. If the heat cannot be transported away from the hydrate core fast enough, the hydrogen bonds will break due to the accumulated heat, and the hydrate core will melt.

The important point here is that any specific case has to be analyzed in detail in terms of coupled mass transport, heat transport, and thermodynamic control (free energy change effect). Then, the appropriate simplifications and approximations can be performed based on physical arguments. Far too often, including examples mentioned here, kinetic models for hydrate phase transitions are based on physically wrong assumptions.

While the kinetic model for hydrate phase transitions presented in this work (CNT) is numerically simple, it still incorporates a newly developed mass transport term based on modern theoretical concepts and results from molecular dynamics simulations. The implicit heat transport model we employ is equally numerically simple but has the advantage of being coupled to a new model for enthalpy calculations completely consistent with the free energies in hydrate and all co-existing phases.

A very important aspect of this work is our use of a thermodynamically consistent approach for all phases: residual thermodynamics. It is slightly outside the main focus of this work to show all the derivations that prove both the consistency and its implications. In brief, the combination of statistical mechanics and classical thermodynamics shows that maintaining the connection between entropy and structure will require consistent calculations of both free energy and enthalpy. That is why it was important for us to demonstrate that our free energy calculations are correct as illustrated by Figure 1 and the comparison with experimental data in our previously published work.

5. Conclusions

Kinetic models found in the literature aiming to describe the kinetics of heterogeneous hydrate film formation and growth are frequently incomplete and lack a fundamental connection to physics-based theoretical platforms. In this work, we propose and demonstrate a theoretical approach able to derive fairly rigorous kinetic models that include implicit coupling between mass transport, heat transport, and phase transition thermodynamic control. We also show that our scheme allows the evaluation of all relevant thermodynamic properties at the same reference level (ideal gas) for all components in all the phases, enthalpies of hydrate formation and dissociation included.

There is a consensus in the available literature that heat transport in aqueous and hydrate systems will be substantially faster than mass transport. An important consequence of this fact is that any kinetic theory of hydrate nucleation, growth, and dissociation has to be based on comprehensive kinetic models incorporating all the implicit coupling mentioned above. Approximations and simplifications must be based on physical reasoning. We have illustrated these points using a realistic representation of the interface between hydrate and liquid. A frequent misunderstanding found in the literature is that hydrate nucleation times can be measured in hours. This confusion is based on visual observations of hydrates which yields the induction time, i.e., time to onset of massive hydrate growth rather than nucleation. Our results calculated basing on the classical nucleation theory indicate that nucleation will occur on the nanoscale, both in respect to time and critical radius dimensions for both heterogeneous and homogeneous hydrate formation from water and dissolved CO_2. On the other hand, the diffusion of hydrate formers across the newly formed hydrate film will be a very slow process responsible for the very lengthy interval before hydrate can be observed on the macroscopic scale. Based on all these observations, we highly recommended that all hydrate kinetic modeling should be based on a sound theoretical foundation. Classical nucleation theory, as utilized in this work, has proven fast enough to be implemented into reservoir simulations. Similar arguments apply to the multicomponent diffusive interface theory (MDIT), which is also very simple numerically. On the other hand, the Phase Field Theory (PFT) lies at the opposite end of the spectrum, being quite numerically intensive for integration at the pore scale level, but the heat transport aspects discussed in this work will also be useful as extensions to our PFT theory for detailed mechanistic studies.

Author Contributions: All authors have contributed to theoretical development, the writing of the paper and analysis of data, including comparisons with experimental data and scientific discussion. All authors have read and agreed to the published version of the manuscript.

Funding: The Research Council of Norway and industrial partners through the following projects: CLIMIT "Safe long term sealing of CO_2 in hydrate," Research Council of Norway project number 224857; SSC-Ramore, "Subsurface storage of CO_2 e Risk assessment, monitoring and remediation," project number: 178008/I30; PETROMAKS "CO_2 injection for extra production," Research Council of Norway project number 801445; PETROMAKS "CO_2 Injection for Stimulated Production of Natural Gas," Research Council of Norway project numbers 175968 and 230083; and STATOIL, under contract 4502354080.

Data Availability Statement: No electronic supplements, refer to the corresponding author for additional details.

Acknowledgments: We acknowledge the grants and support from the NFR and Equinor.

Conflicts of Interest: The authors declare that there are no conflict of interest.

Nomenclature

C	[molecules/Å^3]	Concentration
D	[m^2·s]	Diffusivity
T	[K]	Temperature
Tc	[K]	Critical temperature [K]
Y	[bar or kPa]	Pressure
H	[-]	Hydrate phase
ΔG	[-]	Free energy change
G	[kJ/mol]	Free energy change
H	[-]	Hydrate phase
J	[mol/m^2·s]	Mass transfer Flux
R	[Å]	Distance from liquid side
X	[-]	Mol fraction of liquid
Y	[-]	Mol fraction of gas
Special characters		
Hij	[-]	Canonical cavity partition function of component j in the cavity i
Δgincij	[-]	Free energy of inclusion of the guest molecules jin the cavity i
μ	[kJ/mol]	Chemical potential
∅	[-]	∅ Fugacity coefficient
Γ	[-]	Activity coefficient
Θij	[-]	θij Filling fraction of component j in cavity type i
B	[-]	Inverse of gas constant times temperature
xT	[-]	Total mol fraction of all guests in the hydrate
Subscripts		
H		Hydrate phase
M		Minerals
N		Hydrate Components
P		Parent phase
T		Total
0		Ambient or reference

References

1. Sloan, E.D. Fundamental principles, and applications of natural gas hydrates. *Nature* **2003**, *426*, 353–363. [CrossRef] [PubMed]
2. Kuhs, W.F.; Chazallon, B.; Klapproth, A.; Pauer, F. Filling isotherms in clathrate hydrates. *Rev. High Press. Sci. Technol.* **1998**, *7*, 1147–1149. [CrossRef]
3. Lee, H.; Seo, Y.; Seo, Y.-T.; Moudrakovski, I.L.; Ripmeester, J.A. Recovering Methane from Solid Methane Hydrate with Carbon Dioxide. *Angew. Chem. Int. Ed.* **2003**, *115*, 5202–5205. [CrossRef]
4. Falenty, A.; Genov, G.; Hansen, T.C.; Kuhs, W.F.; Salamatin, A.N. Kinetics of CO_2-Hydrate Formation from Water Frost at Low Temperatures: Experimental Results and Theoretical Model. *J. Phys. Chem. C* **2010**, *115*, 4022–4032. [CrossRef]
5. Kvamme, B.; Kuznetsova, T.; Stensholt, B.J.S.; Bauman, B.; Sjøblom, S.; Lervik, K.N. Consequences of CO_2 solubility for hydrate formation from carbon dioxide containing water and other impurities. *Phys. Chem. Chem. Phys.* **2014**, *16*, 8623–8638. [CrossRef] [PubMed]
6. Kvamme, B.; Kuznetsova, T.; Kivelæ, P.H.; Bauman, J. Can hydrate form in carbon dioxide from dissolved water. *Phys. Chem. Chem. Phys.* **2013**, *15*, 2063–2074. [CrossRef]
7. Kvamme, B.; Tanaka, H. Thermodynamic Stability of Hydrates for Ethane, Ethylene, and Carbon Dioxide. *J. Phys. Chem.* **1995**, *99*, 7114–7119. [CrossRef]
8. Shindo, Y.; Fujioka, Y.; Yanagishita, Y.; Hakuta, T.; Komiyama, H. Formation, and stability of CO2 hydrate. In Proceedings of the 2nd International Workshop on Interaction between CO2 and Ocean, Tsukuba-Ibakari, Tsukuba-Ibakari, Japan, 18–22 January 1999; pp. 111–125.
9. Lund, P.C.; Shindo, Y.; Fujioka, Y.; Komiyama, H. Study of the pseudo-steady-state kinetics of CO_2 hydrate formation and stability. *Int. J. Chem. Kinet.* **1994**, *26*, 289–297. [CrossRef]
10. Teng, H.; Kinoshita, C.M.; Masutani, S.M. Hydrate formation on the surface of a CO_2 droplet in high-pressure, low-temperature water. *Chem. Eng Sci.* **1995**, *50*, 559–564. [CrossRef]

11. Sugaya, M.; Mori, Y.H. Behavior of clathrate hydrate formation at the boundary of liquid water and a fluorocarbon in liquid or vapor state. *Chem. Eng. Sci.* **1996**, *51*, 3505–3517. [CrossRef]
12. Hirai, S.; Okazaki, K.; Araki, N.; Yazawa, H.; Ito, H.; Hijikata, K. Transport phenomena of liquid CO_2 in pressurized water flow with clathrate-hydrate at the interface. *Energy Convers. Manag.* **1996**, *37*, 1073. [CrossRef]
13. Mori, Y.H.; Mochizuki, T. Mass transport across clathrate hydrate films a capillary permeation model. *Chem. Eng. Sci.* **1997**, *52*, 3613–3616. [CrossRef]
14. Mori, Y.H. Clathrate Hydrate Formation at the interface between liquid CO_2 and water phases, a review of rival models characterizing hydrate films. *Energy Convers. Manag.* **1998**, *39*, 1537. [CrossRef]
15. Uchida, T.; Ebinuma, T.; Kawabata, J.; Narita, H. Microscopic observations of formation processes of clathrate-hydrate films at an interface between water and carbon dioxide. *J. Cryst. Growth* **1999**, *204*, 348–356. [CrossRef]
16. Mori, Y.H. Estimating the thickness of hydrate films from their lateral growth rates: Application of a simplified heat transfer model. *J. Cryst. Growth* **2001**, *223*, 206–212. [CrossRef]
17. Freer, E.M.; Selim, M.S.; Sloan, E.D. Methane hydrate film growth kinetics. *Fluid Phase Equilib.* **2001**, *185*, 65–75. [CrossRef]
18. Mochizuki, T.; Mori, Y.H. Clathrate-hydrate film growth along water/hydrate former phase boundaries—Numerical heat-transfer study. *J. Cryst. Growth* **2006**, *290*, 642–652. [CrossRef]
19. Mochizuki, T.; Mori, Y.H. Simultaneous Mass and Heat Transfer to/from the Edge of a Clathrate-Hydrate Film Causing its Growth along a Water/Guest-Fluid Phase Boundary. *Chem. Eng. Sci.* **2017**, *171*, 61–75. [CrossRef]
20. Liu, Z.; Li, H.; Chen, L. A New Model of and Insight into Hydrate Film Lateral Growth along the Gas−Liquid Interface Considering Natural Convection Heat Transfer and Baojiang Sun. *Energy Fuels* **2018**, *32*, 2053–2063. [CrossRef]
21. Svandal, A. Modelling Hydrate Phase Transitions Using Mean-Field Approaches. Ph.D. Thesis, University of Bergen, Bergen, Norway, 2006.
22. Svandal, A.; Kvamme, B.; Granasy, L.; Pusztai, T. The influence of diffusion on hydrate growth. In Proceedings of the 1st International Conference on Diffusion in Solids and Liquids, DSL-2005, Aveiro, Portugal, 6–8 July 2005.
23. Soave, G. Equilibrium constants from a modified Redlich-Kwong equation of state. *Chem. Eng. Sci.* **1972**, *27*, 1197–1203. [CrossRef]
24. Kvamme, B. Thermodynamic Limitations of the CO_2/N_2 Mixture Injected into CH_4 Hydrate in the Ignik Sikumi Field Trial. *J. Chem. Eng. Data* **2016**, *3*, 1280–1295. [CrossRef]
25. Kvamme, B.; Aromada, S.A. Risk of Hydrate Formation during the Processing and Transport of Troll Gas from the North Sea. *J. Chem. Eng. Data* **2017**, *62*, 2163–2177. [CrossRef]
26. Baig, K. Nano to Micro Scale Modelling of Hydrate Phase Transition Kinetics. Ph.D. Thesis, University of Bergen, Bergen, Norway, 2017.
27. Kvamme, B.; Qasim, M.; Baig, K. Hydrate phase transition kinetics from Phase Field Theory with implicit hydrodynamics and heat transport. *Int. J. Greenh. Gas Control* **2014**, *29*, 263–278. [CrossRef]
28. Qasim, M. Microscale Modelling of Natural Gas Hydrates in Reservoirs. Ph.D. Thesis, University of Bergen, Bergen, Norway, 2012.
29. Kvamme, B.; Selvåg, J.; Aromada, S.A.; Saeidi, N.; Kuznetsova, T. Methanol as hydrate inhibitor and hydrate activator. *Phys. Chem. Chem. Phys.* **2018**, *20*, 21968–21987. [CrossRef] [PubMed]
30. Kvamme, B. Enthalpies of hydrate formation from hydrate formers dissolved in water. *Energies* **2019**, *12*, 1039. [CrossRef]
31. Kvamme, B.; Lund, A.; Hertzberg, T. The influence of gas-gas interactions on the Langmuir constants for some natural gas hydrates. *Fluid Phase Equilibria* **1993**, *90*, 15–44. [CrossRef]
32. Kvamme, B.; Førrisdahl, O.K. Polar guest-molecules in natural gas hydrates. *Fluid Phase Equilibria* **1993**, *83*, 427. [CrossRef]
33. Niall, J.E.; John, S.T. Perspectives on Hydrate Thermal Conductivity. *Energies* **2010**, *3*, 1934–1942.
34. Prah, B.; Rin Yun, R. Heat Transfer and Flow Characteristics of CO_2-Hydrate Mixture in Pipeline. *Energy Procedia* **2017**, *114*, 6813–6823. [CrossRef]
35. Sharqawy, M.H.; Lienhard, V.J.H.; Zubair, S.M. Thermophysical properties of seawater: A review of existing correlations and data. *Desalination Water Treat.* **2010**, *16*, 354–380. [CrossRef]
36. Asgeirsson, L.S.; Ghajar, A.J. Prediction of thermal conductivity and Viscosity for some fluids in the near-critical region. *Chem. Eng. Commun.* **1986**, *43*, 165–184. [CrossRef]
37. Todd, B.; Young, J.B. Thermodynamic and transport properties of gases for use in solid oxide fuel cell modelling. *J. Power Sources* **2002**, *110*, 186–200. [CrossRef]
38. Roy, R.F.; Beckand, A.E.; Touloukian, Y.S. Thermophysical Properties of Rocks. *Phys. Prop. Rocks Miner.* **1981**, *198*, 2.
39. Svandal, A.; Kuznetsova, T.; Kvamme, B. Thermodynamic properties and phase transitions in the $H_2O/CO_2/CH_4$ system. *Fluid Phase Equilibria* **2006**, *246*, 177–184. [CrossRef]
40. Tegze, G.; Pusztai, T.; Toth, G.; Granasy, L.; Svandal, A.; Kuznetsova, T.; Buanes, T.; Kvamme, B. Multi-scale approach to CO_2-hydrate formation in aqueous solution. *J. Chem. Phys.* **2006**, *124*, 234710. [CrossRef] [PubMed]
41. Kvamme, B.; Graue, A.; Buanes, T.; Kuznetsova, T.; Ersland, G. Storage of CO_2 in natural gas hydrate reservoirs and the effect of hydrate as an extra sealing in cold aquifers. *Int. J. Green. Gas Control* **2007**, *1*, 236–246. [CrossRef]
42. Kvamme, B.; Aromada, S.A. Alternative routes to hydrate formation during processing and transport of natural gas with significant amount of CO_2: Sleipner gas as a case study. *J. Chem. Eng. Data* **2018**, *63*, 832–844. [CrossRef]
43. Kvamme, B.; Zhao, J.Z.; Wei, N.; Sun, W.T.; Saeidi, N.; Pei, J.; Kuznetsova, T. Hydrate production philosophy and thermodynamic calculations. *Energies* **2020**, *13*, 673. [CrossRef]

44. Kvamme, B. Environmentally friendly production of methane from natural gas hydrate using carbon dioxide. *Sustainability* **2019**, *11*, 1964. [CrossRef]
45. Kvamme, B. Kinetics of Hydrate Formation from Nucleation Theory. *Int. J. Offshore Polar Eng.* **2002**, *12*, 256–263.